Influence of pH and Ionic Strength on the Aggregation Behaviors of Xylan Rich Hemicelluloses with Alkaline Lignins

Guichun Hu,[a,b,c] Jinguang Hu,[c] Honglei Chen,[a] Shunxi Song,[b] and Fuqiang Chu [a]

The evolution of xylan-rich hemicelluloses (XH) aggregation behaviors in the presence of alkaline lignins (AL) under a wide range of pH values and NaCl concentration were investigated *via* dynamic light scattering and turbidity measurements. XH isolated from wheat straw contain a xylose backbone with arabinose side chains and a small amount of phenol groups. XH tend to aggregate in solution due to their low ratio of arabinose to xylose and hydrophobic phenol groups. AL interact with XH through the phenol groups bonded to the hemicellulose main chain to form an AL-XH complex. As the pH value decreases, the particle size and turbidity of AL, XH and their bonded complex all increase. The size of the AL-XH complex agglomerate is greater than the size of a XH at the same pH value, which indicates that the self-assembly of lignin molecules initiate the aggregation of XH. The particle size and turbidity of XH and AL-XH complexes increase as the XH concentration increase. At low pH values, *e.g.*, 6.0, the particle size of the AL-XH complex more obviously increases compared to the XH particles. The size and turbidity of the AL, XH, and AL-XH complex agglomerates increased as the NaCl concentration increased.

Keywords: Xylan rich hemicelluloses; Alkali lignin; Aggregation behavior; pH value; Ionic strength

*Contact information: a: State Key Laboratory of Biobased Material and Green Papermaking, School of Light Industry and Engineering, Qilu University of Technology, Shandong Academy of Sciences, Jinan 250353 P.R. China; b: Key Laboratory of Auxiliary Chemistry and Technology for Chemical Industry, Ministry of Education, Shaanxi University of Science and Technology, Xi'an 710021 P.R. China; c: Department of Chemical and Petroleum Engineering, University of Calgary, Calgary T2N 1N4 Canada; * Corresponding author: hgc-qul@hotmail.com*

INTRODUCTION

Hemicelluloses comprise approximately 15 wt% to 30 wt% of the total lignocellulosic biomass and are the second most abundant renewable source of polysaccharides, after cellulose (Geng *et al.* 2019; Kang *et al.* 2019). Unlike cellulose, which is a homopolysaccharide composed of D-glucose monomers, hemicelluloses are heteropolysaccharides incorporating a variety of sugar units, *e.g.*, glucose, xylose, mannose, galactose, arabinose, fucose, and glucuronic acid (Hu *et al.* 2015; Yu *et al.* 2017; Hu *et al.* 2019; Long *et al.* 2019). These units form a linear backbone heteropolysaccharide with side chains, *e.g.*, arabinoxylan, glucomannan. In a plant cell wall, hemicelluloses are tightly linked with cellulose to form microfibril networks (Yu *et al.* 2017). This natural structure has been applied to manufacture new biomimetic materials (Xu *et al.* 2019; Tedeschi *et al.* 2020).

***bioresources*.com**

Cellulosic fiber integrated with hemicelluloses could greatly enhance the functionalities of the resulting composites, *e.g.*, introducing specific functional groups for the subsequent reaction as well as enhancing the barrier properties and strength properties (Kong *et al.* 2018; Ren *et al.* 2018; Long *et al.* 2019; Pere *et al.* 2019). Hemicelluloses adsorbed on the surface of cellulose perform as aggregates, since hemicellulose aggregates spontaneously, adsorbing on the surface of cellulose in a desorption-resistant manner (Linder *et al.* 2003; Westbye *et al.* 2007; Kanchanalai *et al.* 2016).

Xylan is a predominant type of hemicellulose in plant cell walls, especially in hardwood and herbaceous plants (Shrestha *et al.* 2019). It is characterized by a main chain of β-1,4-linked xylosyl units attached with arabinosyl, glucuronic acid, and acetyl substituents, which contribute to the solubility of xylan in aqueous solutions (Linder *et al.* 2003; Gao *et al.* 2016). It has been reported that xylan is not completely soluble, but tends to aggregate in aqueous solutions (Westbye *et al.* 2007). Two primary factors have been suggested to be responsible for the xylan aggregation: (1) interactions among the linear portions of the hemicellulose main chain, and (2) interactions among the hydrophobic substituents in the hemicellulose main chain, *e.g.*, lignins (phenol groups), bonded to the hemicellulose main chain (Linder *et al.* 2003; Westbye *et al.* 2007). The hydrophobic groups on the hydrophilic main chain are always regarded as a common reason for molecules to aggregate in aqueous solutions (Linder *et al.* 2003; Westbye *et al.* 2007; Evstigneev 2011). Apart from the bonded lignins on the hemicellulose main chain, the unbonded/added lignins have been reported to induce xylan aggregation as well (Westbye *et al.* 2008; Yao *et al.* 2016; Sewring *et al.* 2019). For example, Westbye *et al.* (2008) reported that the addition of isolated lignins increases the agglomeration of xylan and proposed that the possible reason for the agglomeration is the interactions between the lignins and the phenolic substituents attached to the main xylan chain. However, Sewring *et al.* (2019) reported that in the acid precipitation of the kraft lignin process, the added xylan rendered a decrease in the size of the kraft lignin agglomerate.

Lignin itself shows an agglomeration phenomena in aqueous solutions (Evstigneev 2011). The pH value is a key factor in lignin aggregation, and variations in pH have been used for separating lignins from black liquor in the pulp and paper industry. A decrease in the pH value results in an increase in lignin aggregation (Moreva *et al.* 2011; Sewring *et al.* 2019). In addition, ionic strength is an important factor for lignin aggregation. Moreva *et al.* (2011) found that the size of the lignin aggregate was increased with the addition of 0.1 mol/L NaCl. To the best of the knowledge of the authors, no detailed studies can be found in any literatures that monitor the aggregation behavior of xylan in the presence of isolated lignins under a wide range of pH and ionic strength values. In this work, the xylan-rich hemicelluloses (XH) and alkaline lignins (AL) were all isolated from wheat straw with sodium hydroxide. The aggregation behavior of the XH in the presence of AL under a wide range of pH values was investigated *via* particle size distributions at the nano scale, turbidities, and zeta potentials. This indicated that AL interacts with XH through the phenol groups bonded on the XH main chain to form an alkaline lignin-xylan rich hemicellulose (AL-XH) complex and a pH decrease has an important impact on the aggregation behavior of AL-XH complexes. The authors also demonstrated that ionic strength has a more obvious influence on the XH aggregation in the presence of AL than on the XH aggregation without AL.

EXPERIMENTAL

Preparation and Analytical Tests of the Xylan Rich Hemicelluloses (XH) and Alkaline Lignins (AL)

Xylan-rich hemicelluloses were extracted from air-dried wheat straw (harvested from natural stands growing in the south region of the Shandong province, China (N35°42´ 5.03", E118°42´ 40.62")) with aqueous sodium hydroxide, as described in a previous work by the authors (Hu *et al.* 2019). The air-dried wheat straw was ground into powder and then delignified with 6% sodium chlorite under acidic conditions for 3 h. The delignified power was mixed with 5 g/L of sodium hydroxide at a temperature of 30 °C for 10 h. After the suspension was filtered with 400 mesh nylon cloth, the filtrate was neutralized with hydrochloric acid until a pH of 5.5 to 6.0 was reached, and then the solution was centrifuged. The supernatant solution was mixed with triple-volume ethanol. After a centrifugation step, the precipitate was washed with 95% ethanol and dried under a vacuum to obtain the xylan rich hemicelluloses. The XH yield was approximately 10%.

Alkaline lignins were prepared with alkaline extraction followed by acidic precipitation. The air-dried wheat straw (harvested from the Shandong province, China (N35°42' 5.03", E118°42' 40.62")) was ground and screened between 40 mesh and 80 mesh to obtain the powders. Then, the powders were extracted with 12% aqueous sodium hydroxide at a solid-to-liquor ratio of 1 to 12 (g/mL) at a temperature of 80 °C for 2 h. After the suspension was centrifuged at 4000 rpm for 10 min, the supernatant solution was adjusted to a pH of 2 to 2.5 with 1 M HCl and then centrifuged again at 4000 r for 10 min. The precipitate was washed with deionized water until a pH of 5.5 to 6 was reached to obtain alkaline lignin (AL).

The carbohydrate content of the XH and AL was analyzed *via* a Dionex HPLC system (ICS-3000, Dionex Corp., Sunnyvale, CA) equipped with an electrochemical detector and a PA20 column after a two-step hydrolysis with 72% and 4% sulfuric acid (Hu *et al.* 2015). The acid insoluble lignins, acid soluble lignins, and ash in the AL and XH samples were carried out following the appropriate TAPPI standards. The XH and AL were processed according to the following standards: T 222 om-98 (2000) for acid insoluble lignins, T UM 250 (1991) for acid soluble lignins, and T 211 om-02 (2002) for ash.

Preparation of Alkaline Lignin-Xylan Rich Hemicellulose (AL-XH) Complex Solutions

The XH were dissolved in deionized water to obtain a final concentration of 8 g/L and then diluted to different concentrations (0.5 g/L, 1.0 g/L, 1.5 g/L, 2.0 g/L, 3 g/L, 4 g/L, and 5 g/L). The AL were dissolved in 1 M NaOH at room temperature for 4 h to obtain a concentration of 3 mg/mL. To prepare the AL-XH complex solution samples, 5 mL of the XH solution and deionized water were transferred to a test tube denoted sample and then 1 mL of the AL solution (3 g/L) and the appropriate amount of NaCl were added to each of the sample tubes. All the AL-XH complex solution sample tubes were carefully shaken every 30 min for 4 h to ensure the macromolecules mixed thoroughly. For the pure AL solution samples, 1 mL of AL solution (3 g/L) and an appropriate amount of deionized water were added to a test tube, followed by the appropriate amount of NaCl. For pure the XH solution samples, 5 mL of the XH solution, 1 mL of the 1 M NaOH solution, deionized water, and an appropriate amount of NaCl were mixed in a test tube. All samples (AL solution sample, XH solution sample, and AL-XH complex solution sample) were adjusted to the appropriate pH value with 1 M HCl or 1 M NaOH and finally diluted to a total

volume of 10 mL. Finally, the pH value of the diluted mixture was measured. The pH value, AL concentration, XH concentration, and NaCl concentration in AL, XH, and AL-XH complex solutions samples are shown in Table 1.

Table 1. The pH Value, AL Concentration, XH Concentration, and NaCl Concentration in AL, XH, and AL-XH Complex Solutions Samples

Samples	pH value	AL concentration, g/L	XH concentration, g/L	NaCl concentration, M
AL	3.0-13.8	0.3	0	0
XH-1	3.0-13.8	0	0.5	0
AL-XH-1	3.0-13.8	0.3	0.5	0
pH 13.8 XH	13.8	0.0	0.0-4.0	0.0
pH 6.0 XH	6.0	0.0	0.0-4.0	0.0
pH 13.8 AL-XH	13.8	0.3	0.0-4.0	0.0
pH 6.0 AL-XH	6.0	0.3	0.0-4.0	0.0
pH 13.8 AL-X	13.8	0.3	0.0	0.0- 1.0
pH 6.0 AL-X	6.0	0.3	0.0	0.0- 1.0
pH 13.8 XH-5-X	13.8	0.0	2.5	0.0- 1.0
pH 6.0 XH-5-X	6.0	0.0	2.5	0.0- 1.0
pH 13.8 AL-XH-5-X	13.8	0.3	2.5	0.0- 1.0
pH 6.0 AL-XH-5-X	6.0	0.3	2.5	0.0- 1.0
pH 13.8 AL	13.8	0.3	0.0	0.0
pH 6.0 AL	6.0	0.3	0.0	0.0
pH 13.8 XH-1	13.8	0.0	0.5	0.0
pH 13.8 XH-5	13.8	0.0	2.5	0.0
pH 6.0 XH-1	6.0	0.0	0.5	0.0
pH 6.0 XH-5	6.0	0.0	2.5	0.0
pH 13.8 AL-XH-1	13.8	0.3	0.5	0.0
pH 13.8 AL-XH-5	13.8	0.3	2.5	0.0
pH 6.0 AL-XH-1	6.0	0.3	0.5	0.0
pH 6.0 AL-XH-5	6.0	0.3	2.5	0.0
pH 13.8 AL-N	13.8	0.3	0.0	0.8
pH 6.0 AL-N	6.0	0.3	0.0	0.8
pH 13.8 XH-5-N	13.8	0.0	2.5	0.8
pH 6.0 XH-5-N	6.0	0.0	2.5	0.8
pH 13.8 AL-XH-5-N	13.8	0.3	2.5	0.8
pH 6.0 AL-XH-5-N	6.0	0.3	2.5	0.8

Size and Zeta Potential

The size and zeta potential of the AL, XH, and AL-XH complex as a function of pH and ionic strength were measured at 633 nm *via* a DLS (dynamic light scattering) analyzer equipped with a laser Doppler microelectrophoresis (Zetasizer Nano ZS90, Malvern Instruments, Malvern, United Kingdom).

Turbidity Measurement

The turbidity was measured *via* a UV-VIS-spectrophotometer at 500 nm according to Westbye *et al.* (2007). The turbidity was calculated according to Eq. 1,

$$Turbidity = \frac{Absorbance}{Pathlength} \times \ln 10 \tag{1}$$

where absorbance is the sample absorbance at 500 nm and the pathlength is the light path in the sample was 1 cm. All the samples were analyzed *via* UV-VIS-spectrophotometer with 10 mL of a water-NaOH mixture solution (deionized water, 1 mL of 1 M NaOH solution, and an appropriate amount of NaCl) at an appropriate pH value, as a blank.

RESULTS AND DISCUSSIONS

Characterization of the Xylan Rich Hemicelluloses (XH) and the Alkaline Lignins (AL)

The carbohydrate composition and lignin content of the AL and XH were analyzed, and results are shown in Table 2. The dominant carbohydrate of the XH was xylose (Xyl), which contributed to 78% (w/w) of the total neutral sugar content. Arabinose (Ara) was the second most abundant carbohydrate after xylose, which accounted for 16.5% of the total XH weight. The ratio of arabinose to xylose is a key factor in terms of xylan aggregation and weakly substituted xylan tends to aggregate (Hu *et al.* 2015; Liu *et al.* 2017; Ghosh *et al.* 2021). The arabinose to xylose ratio of XH was 0.22, which indicated that the number of side chains along the xylan main chain was low and the number of linear portions in the XH was high. In plant cell walls, xylan strongly interacts with lignins *via* phenyl glycosidic linkage, benzyl ester, and benzyl ether; therefore, it is hard to isolate pure xylan (Westbye *et al.* 2007). In addition, there were also small amounts of acid soluble lignins and acid insoluble lignins in the XH. For the AL fraction, acid insoluble lignins occupied the majority, accounting for 77.9%, with acid soluble lignins the second most numerous, accounting for 15.6% (Table 2). There were still a small amount of carbohydrates and ash.

Table 2. Composition of XH and AL

Fraction	Xyl	Ara	Glu	Gal	Lignin		Ash	Others
					ASL	AIL		
XH	73.9%	16.7%	2.6%	1.3%	3.2%	1.4%	0.2%	0.7%
AL	0.1%	-	0.2%	-	15.6%	77.9%	2.8%	0.4%
Note: values are given in weight percentage of dry samples. Xyl: xylose; Ara: arabinose; Glu: glucose; Gal: galactose; ASL: Acid soluble lignin; and AIL: Acid insoluble lignin.								

The Influences of the pH on the Interactions between Alkaline Lignins (AL) and Xylan Rich Hemicelluloses (XH)

It is well known that pH is a key factor in terms of xylan and lignin agglomeration (Westbye *et al.* 2007; Sewring *et al.* 2019). The influences of the pH on the size distributions, zeta potential, and conductivity of XH and AL were investigated *via* dynamic light scattering (DLS), as shown in Fig. 1. At a pH of 13.8, the size distribution of the AL (concentration 0.3 g/L) had a unimodal distribution with a size range of 80 to 106 nm (Fig. 1a). The phenolic and carboxyl groups of the lignin molecules at high pH values were

dissociated and thus could access the NaOH solution, leading to the lignins dissolving in the aqueous alkali solution (Evstigneev 2011; Sewring *et al.* 2019). When the pH value was decreased to 6.0, the size distribution of the AL aggregates exhibited a bimodal distribution. The small particles were in the range 80 to 142 nm, and the large particles were between 190 and 615 nm, which accounted for 77% of the total particles. The absolute zeta potential of the AL decreased from 25.2 mV to 11.9 mV as the pH decreased from 13.8 to 6.0 (Fig. 1b). A reduction in pH decreased the surface negative charge density of the AL particles and, hence, reduced the ion-electrostatic component of the interparticle interaction energy during the AL dispersions (Moreva *et al.* 2011). In addition, the aggregation of AL also led to the reduction of conductivity. The AL conductivity decreased from 18.2 mS/cm at pH 13.8 to 11.6 mS/cm at pH 6.0. The proposed aggregation mechanism of AL is shown in Fig. 3a and 3b.

The particle size of the XH increased as the pH decreased as well (Fig. 1a). The size distributions of XH-1 (XH concentration of 0.5g/L) at a pH of 13.8 and 6.0 were bimodal. As the pH value was decreased from13.8 to 6.0, the small particles changed from the range of 37 to 79 nm at a pH of 13.8 to the range of 37 to 90 nm at a pH of 6.0 while the large particles increased in size from 106 to 255 nm at a pH of 13.8 to the range of 90 to 531 nm at a pH of 6.0. In addition, the absolute zeta potential and conductivity decreased from 23.2 mV and 20.4 mS/cm at a pH of 13.8 to 8.8 mV and 11.0 mS/cm at a pH of 6.0, respectively. The hydroxyl groups in the XH extend in the solution at a high pH value, which led to the high surface charge. A decrease in the pH to 6.0 suppressed the dissociation of the hydroxyl groups, leading to a reduction in the surface charge of the XH (Shrestha *et al.* 2019). As shown in Table 2, the XH contains not only linear chain parts but lignin groups. As the pH decreases, the linear parts of the XH interact with each other to form hydrogen bonds and the hydrophobic lignin groups bound to the XH main chain aggregate (Figs. 3c and 3d), which lead to the aggregation of XH (Linder *et al.* 2003; Westbye *et al.* 2007).
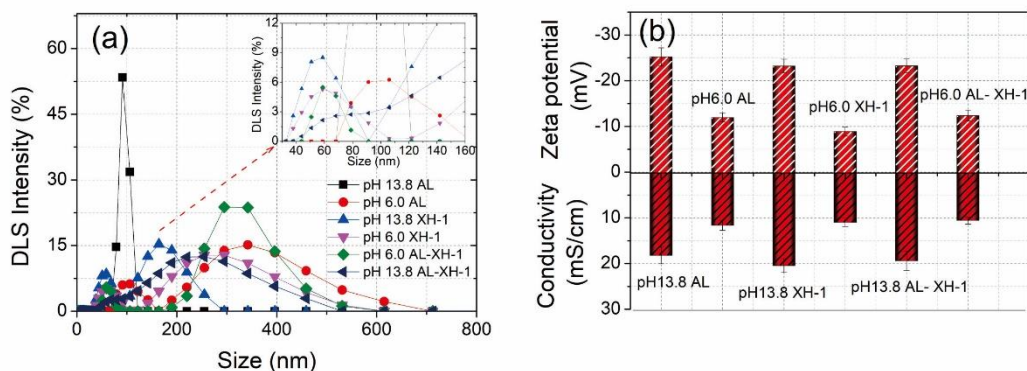

Fig. 1. The size distributions (a) the zeta potentials and conductivities (b) of the XH, AL, and AL-XH complexes at a pH of 13.8 and a pH of 6.0

The particle size variations of the XH and AL complex solution at a pH of 6.0 and 13.8 are shown in Fig. 1a. At a pH of 13.8, the particles of the AL and XH-1 complex solution (0.3g/L of AL and 0.5g/L of XH) ranged from 44 to 459 nm, and they were obviously larger than the particles sizes of the XH-1 and AL aggregates at the same pH value. It has been reported that lignins can interact with the phenolic substituents attached

to the backbone of xylan, forming a xylan and lignin complex (Westbye *et al.* 2007; Sewring *et al.* 2019). Therefore, the authors deduced that in the AL and XH complex solution, the AL connected with the phenolic groups of the XH, forming an AL-XH complex. As the pH value was decreased to 6.0, the particles sizes of the AL-XH-1 complex (in a 0.3g/L of AL and 0.5g/L of XH complex solution) increased, with 85% of the particles ranging from 220 to 531 nm, whereas at same pH value, the XH-1 particle sizes ranged from 90 to 531 nm and only accounted for 78% of the particles. This phenomenon echoes the study by Westbye *et al.* (2007), which has shown that the addition of lignins increases the self-assembly of xylan. As previously discussed, a decrease in pH value increases the aggregations of AL and XH, especially for AL aggregations. During the pH decreasing process, the added AL and phenolic substituents of the XH aggregate initiated the aggregation of an AL-XH complex to form a unique structure with a hydrophobic core, which consisted of aggregated AL surrounded by hydrophilic side chains of XH (Fig. 3e and 3f). In addition, the interactions between the linear chains in the XH is another possible reason for the aggregation of AL-XH (Figs. 3e and 3f). The aggregation of AL-XH complex results in the reduction of absolute zeta potential and conductivity. The absolute zeta potential and conductivity of AL-XH-1 decreased from 23.2 mV and 19.4 mS/cm at pH 13.8 to 12.4 mV and 10.6 mS/cm at pH 6.0, respectively. In addition, the sizes of the AL-XH-1 aggregates were smaller than AL at a pH of 6.0, which indicated that XH disturbs the aggregation of AL. This is consistent with the results of Sewring *et al.* (2019), which also found that xylan disturbs the aggregation of lignins, which leads to a reduction in its aggregate size (Durruty *et al.* 2017).
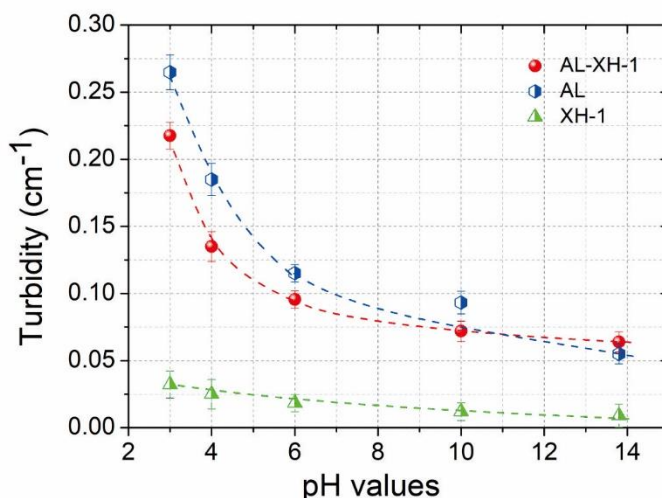

Fig. 2. The influences of the pH on the turbidities of XH-1, AL, and AL-XH-1 complex in solutions

Turbidity is recognized as another reasonable approach to evaluate the aggregation/ self-assemble of polysaccharides or biopolymers in solution (Norgren *et al.* 2002; Westbye *et al.* 2007; Hall *et al.* 2016). When polysaccharides aggregate in solution, the turbidity is high; when no polysaccharides aggregate, the turbidity is low (Norgren *et al.* 2002; Westbye *et al.* 2007; Hall *et al.* 2016). To provide additional insight on XH aggregation behaviors in the presence of AL, the turbidities of the AL, XH, and AL-XH complexes were measured (Fig. 2). The turbidities of the AL, XH, and AL-XH complexes all increased as the pH decreased. The turbidity of XH-1 (a XH concentration of 0.5 g/L) moderately

increased as the pH decreased, which agrees with the particle size variation of XH-1, as shown by the DLS. The turbidity of the AL sharply increased as the pH decreased, especially at pH values greater than 7.0. The turbidity of the AL-XH-1 complex had similar tendencies to AL, whereas the turbidity of the AL-XH-1 complex was smaller than AL at the same pH value, which confirmed the results of the particle size analysis for the AL-XH-1 complex during the pH reduction process.
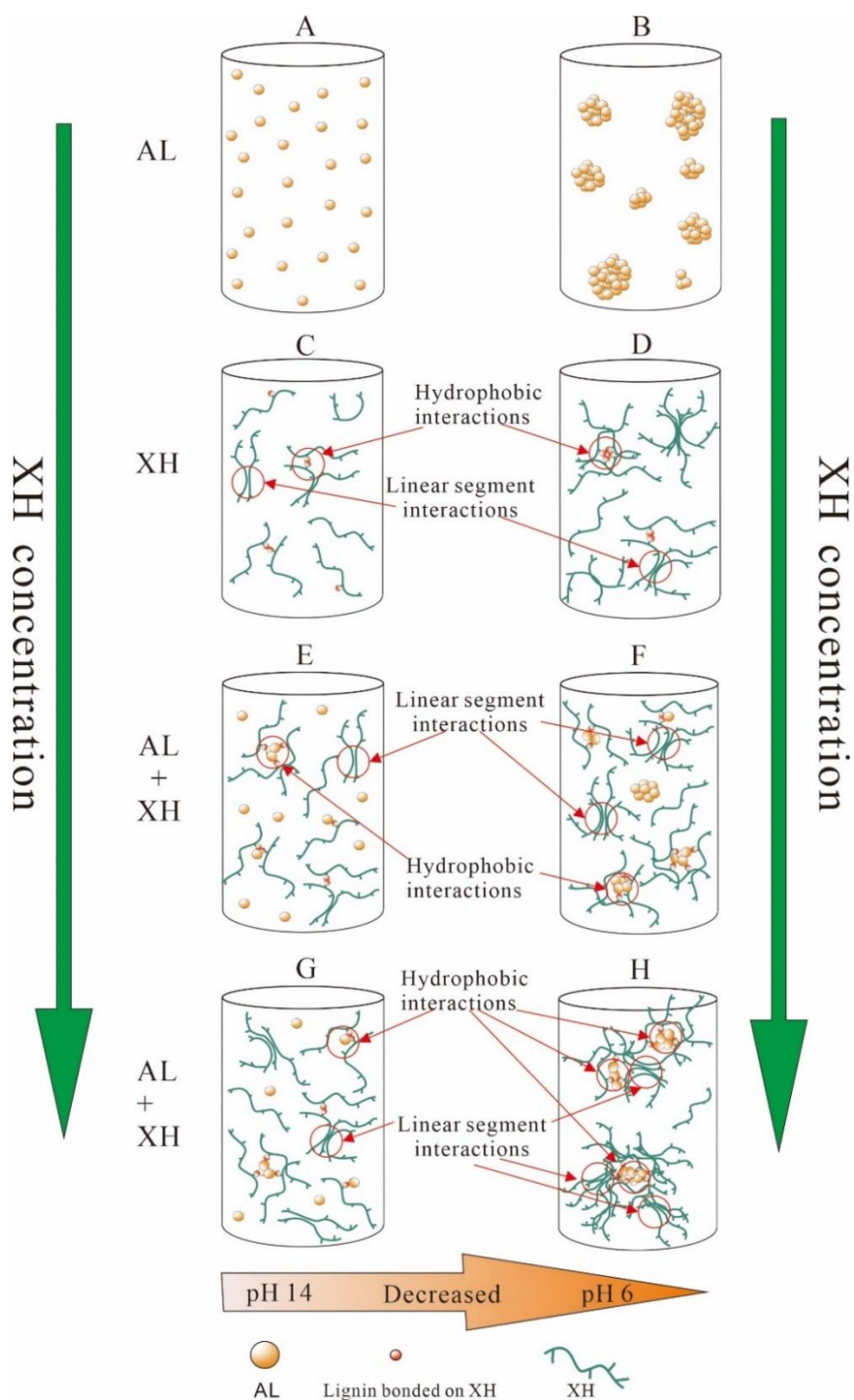

Fig. 3. Proposed aggregation mechanisms of the AL (A,B), the XH (C,D), AL-XH complexes with low amounts of XH (E,F), and AL-XH complexes with adequate XH (E,F)

The Effect of the Xylan Rich Hemicellulose (XH) Concentration on the Alkaline Lignin-Xylan Rich Hemicellulose (AL-XH) Aggregation

In the previous section, it was found that at low XH concentrations, the addition of AL enhanced the aggregation of XH, causing the formation of AL-XH complexes as the pH decreased. However, the influences of a high XH concentration on AL-XH complex aggregation are unknown. The turbidities of the AL-XH complexes depended on the XH concentration at a pH of 13.8 and 6.0 are shown in Fig. 4. The turbidities of the XH and AL-XH complexes at a pH of 6.0 and 13.8 all increased as the concentration of XH increased. With the increase in XH concentration, the turbidities of the AL-XH complexes more obviously increased compared to XH at the same pH value. For instance, when the XH concentration was increased from 0.25 g/L to 4 g/L, the turbidity of the AL-XH complexes at a pH of 6.0 increased by 523%, whereas, at the same pH value, the turbidity of XH increases by 469%. In addition, the turbidities of the AL-XH complexes at a pH of 6.0 and 13.8 were higher than the theoretical turbidities of the AL-XH complexes at XH concentrations greater than 1.5 g/L and 0.75 g/L, respectively. This indicated that the increase in XH concentration enhanced the aggregation of AL-XH complexes. A possible reason is that the increase in XH concentration facilitates aggregation of XH molecules. The present of AL enhances the aggregation of XH and AL-XH complex. The theoretical turbidities of the AL-XH complexes with the method adopted from Westbye *et al.* (2007) is the theoretical combination of AL and XH.
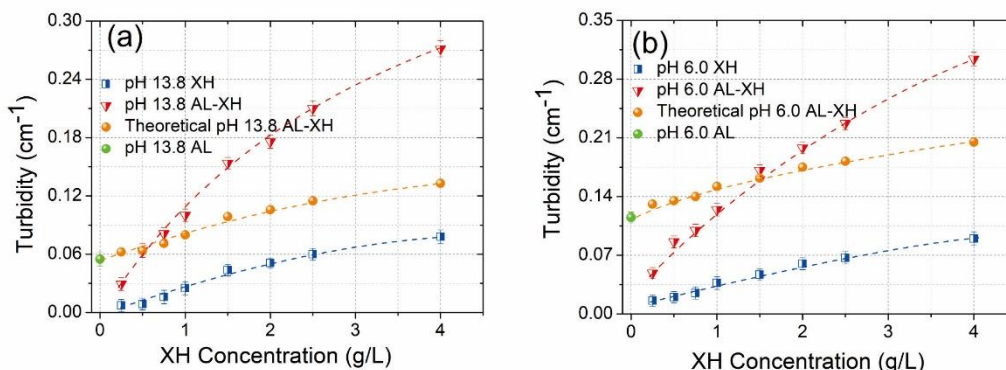

Fig. 4. The effects of the XH concentration on the turbidities of XH and the AL-XH complex aggregates at pH values of 13.8 (a) and 6.0 (b). (Theoretical pH 6.0 AL-XH and theoretical pH 13.8 AL-XH: theoretical turbidities of AL-XH complex solution at pH 6.0 and pH 13.8, respectively)

The size distributions of the XH-5 aggregates (a XH concentration of 2.5 g/L) and the AL-XH complexes with 2.5 g/L of XH (abbreviated AL-XH-5) at a pH of 13.8 and 6.0 were investigated (Fig. 5). The size of the XH aggregates increased as the XH concentration increased. At a pH of 13.8, the size of the XH-5 aggregates ranged from 43 nm to 396 nm, which were larger than the XH-1 aggregates (a XH concentration of 0.5 g/L). At a pH of 6.0, the XH-5 aggregates that ranged from 220 nm to 531 nm was as high as 79%, whereas the size of XH-1 aggregates in that range only accounted for 61% of the distribution. A possible reason for this is that the increase in XH concentration promotes interactions between the XH molecules. The decrease in pH increases the collision opportunities of the XH aggregates, thus forming the large XH aggregates.

The increase in XH concentration increased the particle size of the AL-XH complexes, which echoes the turbidity changes of the AL-XH complexes. The size

distribution of the AL-XH-5 complex (an AL-XH complex solution with 2.5 g/L of XH and 0.3 g/L of AL) at a pH of 13.8 was bimodal and portions of the particles reached as big as 615 nm, whereas the largest particle size of the AL-XH-1 complex (an AL-XH complex with 0.5 g/L of XH and 0.3 g/L of AL) at a pH of 13.8 was 459 nm. At a pH of 6.0, the size of the AL-XH-5 complex aggregates ranged from 80 to 712 nm, with the particles ranging from 396 to 712 nm comprising as high as 71% of the distribution; the number of particles in the AL-XH-1 complex larger than 396 nm was only 20%. In addition, at the same pH, the particle size of the AL-XH-5 complex was larger than the AL particle size, which was consistent with the turbidity change in the AL-XH complexes as the XH concentration increased. The absolute zeta potential of the AL-XH-5 complex was lower than the absolute zeta potential of the AL-XH-1 complex at the same pH value. The absolute zeta potentials of the AL-XH-5 complex and the AL-XH-1 complex at a pH of 13.8 were 18 and 23 mV, respectively. The increase in XH concentration in the AL and XH complex solution formed not only the AL-XH complex aggregates, but XH aggregates as well. As the pH was decreased, the collisions between the XH and AL-XH complex aggregates increased, thus causing more disordered and loosely bounded aggregates, leading to an increased in the particle sizes of the XH and AL-XH complexes (Figs. 3g and 3h).
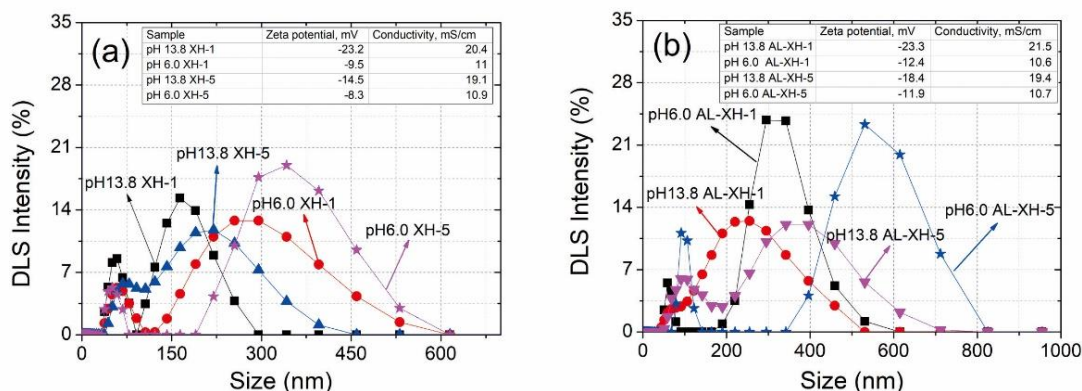

Fig. 5. The effect of the XH concentration on the size distribution, zeta potential, and conductivity of the XH (a) and the AL-XH complex (b) aggregates

The Effect of the Ionic Strength on the Alkaline Lignin-Xylan Rich Hemicellulose (AL-XH) Aggregation

It has been shown that ionic strength has a considerable influence on the aggregation of lignins and xylans since the electrostatic repulsion between the charged entities is strongly screened, causing the balance between the attractive forces and electrostatic repulsion to break (Norgren *et al.* 2001, 2002; Westbye *et al.* 2007; Moreva *et al.* 2011). The influences of the NaCl concentration on the turbidities of XH and AL, as well as the AL-XH complexes, are shown in Fig. 6. The turbidities of AL, XH, and the AL-XH complexes increased as the NaCl concentration increased, but the effects of the NaCl concentration are different. The turbidities of the AL (0.3g/ L) at a pH of 13.8 and a pH of 6.0 reached the balance values at 0.2 M of NaCl and 0.4 M of NaCl, respectively. The turbidities of XH (a concentration of 2.5g/ L) at a pH of 13.8 and 6.0 slightly increased as the NaCl concentration increased, and all reached the balance values at 0.2 M of NaCl. For the AL-XH complexes (with 2.5g/ L of XH and 0.3g/ L of AL), the turbidity at a pH of 13.8 reached equilibrium value at 0.2 M of NaCl, whereas at a pH of 6.0, the equilibrium

turbidity of the AL-XH complexes was reached at 0.6 M of NaCl. This indicated that compared to both AL and XH, a high NaCl concentration was needed to reach the equilibrium turbidity of the AL-XH complexes at a low pH value.
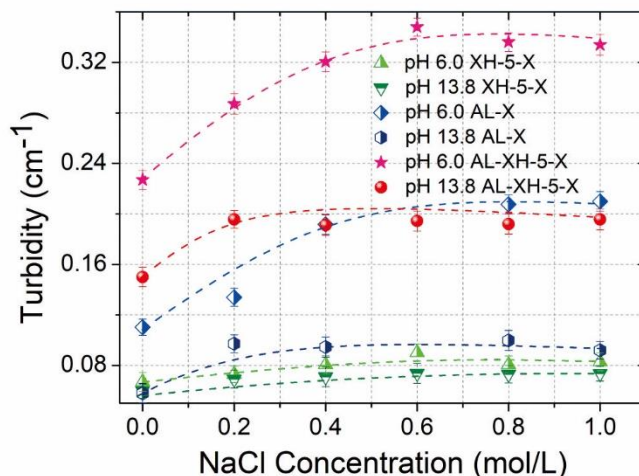

Fig. 6. The effects of the NaCl concentration on the turbidity of the XH, AL, and the AL-XH complexes

The influences of the NaCl concentration (0.8 mol/L of NaCl) on the size distributions of AL, XH, and the AL-XH complexes at a pH of 6.0 and 13.8 were investigated (Fig. 7).
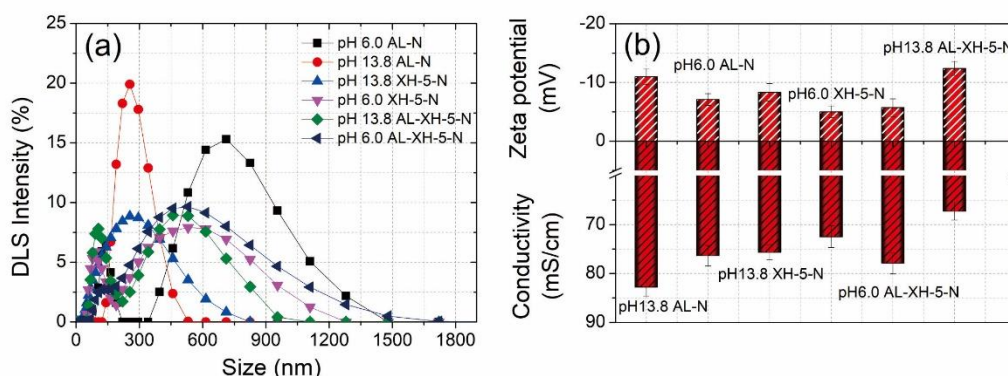

Fig. 7. The influence of the ion strength on the size distribution (a) and zeta potential and conductivity (b) of the XH, AL, and the AL-XH complexes

The particle sizes of AL and XH all increased with the addition of NaCl. The particle size of AL-N (0.3g/L of AL solution with 0.8 mol/L of NaCl) at a pH of 13.8 ranged from 142 to 531 nm and were larger than the AL particles (between 78 and 106 nm) at the same pH value without NaCl. When the pH was decreased to 6.0, the particles of AL-N increased, with 79% of the particles ranging between 396 and 1280 nm, which were obviously larger than the AL particles at the same pH value without NaCl (as shown in Fig.

1). Similarly, the particle size of XH-5-N (2.5g/ L of XH solution with 0.8 mol/L of NaCl) at a pH of 13.8 increased to 712 nm and were larger than the XH particles (2.5g/ L of XH) at the same pH value without NaCl. When the pH was decreased to 6.0, the particles of XH-5-N increased, with 65% particles ranging between 190 and 1100 nm, which were much larger than the XH particles (2.5g/ L of XH) at a pH of 6.0 without NaCl. A possible reason for this is that the addition of NaCl causes the compression of electrical double layers and a decrease in the energy barrier, which consequently causes a decrease in the aggregation stability of the system (Moreva *et al.* 2011).

It can be seen from Fig. 7 that the particles of the AL-XH-5-N complex (a 2.5 g/L of XH and 0.3 g/L of AL complex solution with 0.8 M of NaCl) at a pH of 13.8 and a pH of 6.0 were much larger than the AL-XH-5 complex particles (2.5 g/L of XH and 0.3 g/L of AL) without the addition of NaCl (Fig. 5). As the pH was decreased to 6.0, the effects of NaCl became more obvious. At a pH of 6.0, the AL-XH-5-N complex particles ranging between 190 and 1720 nm accounted for 86% of the distribution, which was much greater than the AL-XH-5 complex particles without the addition of NaCl. The absolute zeta potentials of the AL-XH-5-N complex were lower than the AL-XH-5 complex without the addition of NaCl. The zeta potentials of the AL-XH-5-N complex at a pH of 6.0 and 13.8 were -9 and -5 mV, respectively, whereas the zeta potentials of the AL-XH-5 complex at a pH of 6.0 and 13.8 were -18 and -12 mV, respectively. A possible reason for this is that the addition of NaCl decreases the stability of the AL-XH complexes, which changes the AL-XH complex cluster structure into the larger AL-XH complex structure *via* aggregation. Due to the presence of sodium and chloride, the conductivities of AL-N, XH-5-N, and AL-XH-5-N with 0.8 mol/L of NaCl were higher than the AL, XH-5, and AL-XH-5 samples, respectively.

CONCLUSIONS

1. Xylan rich hemicelluloses (XH) isolated from wheat straw primarily contains xylose and arabinose as well as a small amount of lignins (phenol groups). The low ratio of arabinose to xylose and hydrophobic phenol groups in XH makes it easy to self-assemble.

2. The particle sizes and turbidities of XH and AL increased as the pH decreased, which indicated that the change in pH value greatly affected the aggregation of XH and AL. In addition, the particle size of XH was larger than the particle size of AL at the same pH value.

3. In a XH and AL complex solution, the AL interacted with the phenol groups on the main chain of the XH to form an AL-XH aggregation complex. The turbidity and particle size of the AL-XH complexes increased as the pH decreased and the particle size of the AL-XH complexes was larger than the particle size of XH at the same pH. The aggregations of added AL and the phenol groups on XH insulated the aggregation of the AL-XH complexes.

4. The aggregation of XH and the AL-XH complexes increased as the XH concentration increased, which lead to the increases in their particle size and turbidity. With a reduction in pH, the particle size of the AL-XH complexes more obviously increased compared to the XH particles.

5. At low XH concentrations, *e.g.*, 0.5 g/L, the size of the AL-XH complex agglomerates were small compared to the AL agglomerates. When the XH concentration increased above a certain concentration, which was dependent on the pH value, the size of the AL-XH complex agglomerates were larger than the size of the AL agglomerates.

6. Ionic strength is an important factor in terms of the aggregate formation of AL and XH, as well as AL-XH complexes. The NaCl concentration was found to induce dramatic effects on the aggregation of AL and AL-XH complexes. The effect of the NaCl concentration on the aggregation of AL-XH complexes was more obvious compared to the aggregation of AL and XH, especially at low pH values.

ACKNOWLEDGEMENTS

REFERENCES CITED

Durruty, J., Mattsson, T., and Theliander, H. (2017). "Local filtration properties of Kraft lignin: The influence of residual xylan," *Separation and Purification Technology* 179, 455-466. DOI: 10.1016/j.seppur.2017.01.068

Evstigneev, E. I. (2011). "Factors affecting lignin solubility," *Macromolecular Chemistry and Polymeric Materials* 84(6), 1019-1024. DOI: 10.1134/S1070427211060243

Gao, C., Ren, J., Zhao, C., Kong, W., Dai, Q., Chen, Q., Liu, C., and Sun, R. (2016). "Xylan-based temperature/pH sensitive hydrogels for drug controlled release," *Carbohydrate Polymers* 151, 189-197. DOI: 10.1016/j.carbpol.2016.05.075

Geng, W., Narron, R., Jiang, X., Pawlak, J. J., Chang, H., Park, S., Jameel, H., and Venditti R. A. (2019). "The influence of lignin content and structure on hemicelluloses alkaline extraction for non-wood and hardwood lignocellulosic biomass," *Cellulose* 26, 3219-3230. DOI: 10.1007/s10570-019-02261-y

Ghosh, D., Tanner, J., Lavoie, J.-M., Garnier, G., and Patti, A. F. (2021). "An integrated approach for hemicellulose extraction from forest residue," *BioResources* 16(2), 2524-2547. DOI: 10.15376/biores.16.2.2524-2547

Hall, D., Zhao, R., Dehlsen, I., Bloomfield, N., Williams, S. R., Arisaka, F., Goto, Y., and Carver, J. A. (2016). "Protein aggregate turbidity: Simulation of turbidity profiles for mixed aggregation reactions," *Analytical Biochemistry* 498, 1-17. DOI: 10.1016/j.ab.2015.11.021

Hu, G., Fu, S., Liu, H., and Lucia, L. A. (2015). "Adsorption of cationized eucalyptus heteropolysaccharides onto chemical and mechanical pulp fibers," *Carbohydrate Polymers* 123, 324-330. DOI: 10.1016/j.carbpol.2015.01.057

Hu, G.-C., Fu, S., Chu, F., and Wu, G. (2019). "Fabrication of an all-polysaccharide composite film from hemicellulose and methylcellulose," *BioResources* 14(3), 716-6726. DOI: 10.15376/biores.14.3.6716-6726

Kanchanalai, P., Temani, G., Kawajiri, Y., and Realff, M. J. (2016). "Reaction kinetics of concentrated-acid hydrolysis for cellulose and hemicellulose and effect of crystallinity," *BioResources* 11(1), 1672-1689. DOI: 10.15376/biores.11.1.1672-1689

Kang, X., Kirui, A., Widanage, M. C. D., Mentink-Vigier, F., Cosgrove, D. J., and Wang, T. (2019). "Lignin-polysaccharide interactions in plant secondary cell walls revealed by solid-state NMR," *Nature Communications* 10, 1-9. DOI: 10.1038/s41467-018-08252-0

Kong, F., Guo, Y., Liu, Z., Wang, S., and Lucia, L. A. (2018). "Synthesis of cationic xylan derivatives and application as strengthening agents in papermaking," *BioResources* 13(2), 2960-2976. DOI: 10.15376/biores.13.2.2960-2976

Linder, A., Bergman, R., Bodin, A., and Gatenholm, P. (2003). "Mechanism of assembly of xylan onto cellulose surfaces," *Langmuir* 19(12), 5072-5077. DOI: 10.1021/la0341355

Liu, Z., Wang, L., Zhang, Y., Li, Y., Li, Z., and Cai, H. (2017). "Cellulose-lignin and xylan-lignin interactions on the formation of lignin-derived phenols in pyrolysis oil," *BioResources* 12(3), 4958-4971. DOI: 10.15376/biores.12.3.4958-4971

Long, L., Shen, F., Wang, F., Tian, D., and Hu, J. (2019). "Synthesis, characterization and enzymatic surface roughing of cellulose/xylan composite films," *Carbohydrate Polymers* 213, 121-127. DOI: 10.1016/j.carbpol.2019.02.086

Moreva, Y. L., Alekseeva, N. S., and Chernoberezhskii, Y. M. (2011). "Influence of NaOH, HCl, NaCl, and $CaCl_2$ electrolytes on aggregation stability of aqueous craft lignin dispersion according to data of filtration through track membranes," *Colloid Journal* 73(3), 363-367. DOI: 10.1134/S1061933X11030082

Norgren, M., Edlund, H., and Wågberg, L. (2002). "Aggregation of lignin derivatives under alkaline conditions. Kinetics and aggregate structure," *Langmuir* 18(7), 2859-2865. DOI: 10.1021/la011627d

Norgren, M., Edlund, H., Wagberg, L., Lindstrom, B., and Annergren, G. (2001). "Aggregation of Kraft lignin derivatives under conditions relevant to the process, Part I. Phase behaviour," *Colloids and Surfaces A: Physicochemical and Engineering Aspects* 194(1-3), 85-96. DOI: 10.1016/S0927-7757(01)00753-1

Pere, J., Pääkkönen, E., Ji, Y., and Retulainen, E. (2019). "Influence of the hemicellulose content on the fiber properties, strength, and formability of handsheets," *BioResources* 14(1), 251-263. DOI: 10.15376/biores.14.1.251-263

Ren, J., Dai, Q., Zhong, H., Liu, X., Meng, L., Wang, X., and Xin, F. (2018). "Quaternized xylan/cellulose nanocrystal reinforced magnetic hydrogels with high strength," *Cellulose* 25, 4537-4549. DOI: 10.1007/s10570-018-1858-4

Sewring, T., Durruty, J., Schneider, L., Schneider, H., Mattsson, T., and Theliander, H. (2019). "Acid precipitation of kraft lignin from aqueous solutions: The influence of pH, temperature, and xylan," *Journal of Wood Chemistry and Technology* 39(1), 1-3. DOI: 10.1080/02773813.2018.1488870

Shrestha, U. R., Smith, S., Pingali, S. V., Yang, H., Zahran, M., Breunig, L., Wilson, L. A., Kowali, M., Kubicki, J. D., Cosgrove, D. J., *et al.* (2019). "Arabinose substitution effect on xylan rigidity and self-aggregation," *Cellulose* 26, 2267-2278. DOI: 10.1007/s10570-018-2202-8

TAPPI (US Technical Association of Pulp and Paper Industry) Test Methods T211 om-02. (2002). "Ash in wood, pulp, paper and paperboard: Combustion at 525 °C," TAPPI Press, Atlanta, GA.

TAPPI (US Technical Association of Pulp and Paper Industry) Test Methods T222 om-

    98. (2000). "Acid-insoluble lignin in wood and pulp," TAPPI Press, Atlanta, GA.
TAPPI (US Technical Association of Pulp and Paper Industry) Useful Test Methods UM
    250. (1991). "Acid-soluble lignin in wood and pulp," TAPPI Press, Atlanta, GA.
Tedeschi, G., Guzman-Puyol, S., Ceseracciu, L., Paul, U. C., Picone, P., Carlo, M. D.,
    Athanassiou, A., and Heredia-Guerrero, J. A. (2020). "Multifunctional bioplastic
    inspired by wood composition: Effect of hydrolyzed lignin addition to xylan-cellulose
    matrice," *Biomacromolecules* 21(2), 910-920. DOI: 10.1021/acs.biomac.9b01569
Westbye, P., Köhnke, T., and Gatenholm, P. (2008). "Fraction and characterization of
    xylan rich extracts from birch," *Holzforschung* 62, 31-37. DOI:
    10.1515/HF.2008.005.
Westbye, P., Köhnke, T., Glasser, W., and Gatenholm, P. (2007). "The influence of
    lignin on the self-assembly behaviour of xylan rich fractions from birch (*Betula
    pendula*)," *Cellulose* 14, 603-613. DOI: 10.1007/s10570-007-9178-0
Xu, J., Xia, R., Zheng, L., Yuan, T., and Sun, R. (2019). "Plasticized hemicelluloses/
    chitosan-based edible films reinforced by cellulose nanofiber with enhanced
    mechanical properties," *Carbohydrate Polymers* 224, 115164. DOI:
    10.1016/j.carbpol.2019.115164
Yao, L., Chen, C., Zheng, X., Peng, Z., Yang, H., and Xie, Y. (2016). "Determination of
    lignin-carbohydrate complexes structure of wheat straw using carbon-13 isotope as a
    tracer," *BioResources* 11(3), 6692-6707. DOI: 10.15376/biores.11.3.6692-6707
Yu, J., Paterson, N., Blamey, J., and Millan, M. (2017). "Cellulose, xylan and lignin
    interactions during pyrolysis of lignocellulosic biomass," *Fuel* 191, 140-149. DOI:
    10.1016/j.fuel.2016.11.057